# Dimensional synthesis and dynamic manipulability of a planar two-degree-of-freedom parallel manipulator

**J Wu***, **J Wang, L Wang,** and **H Shao**
Institute of Manufacturing Engineering, Department of Precision Instruments, Tsinghua University, Beijing, People's Republic of China

*The manuscript was received on 22 August 2007 and was accepted after revision for publication on 24 January 2008.*

DOI: 10.1243/09544062JMES830

**Abstract:** This article deals with the dimensional synthesis and dynamic manipulability of a planar two-degree-of-freedom (DOF) parallel manipulator. The dimensional synthesis based on the workspace and velocity output ratio is presented. The dynamic formulation is derived by using the virtual work principle. Taking into account that the accelerating capabilities at a given point along all directions are more isotropic, the condition number of inertia matrix in the dynamic equation is presented as an index to evaluate the dynamic manipulability of a manipulator. Furthermore, two global performance indices, which consider the mean value and standard deviation of the condition number of inertia matrix, are proposed, respectively. The dynamic manipulability of the parallel manipulator is more isotropic in the centre than at the peripheries of the workspace. The parallel manipulator is incorporated into a four-DOF hybrid machine tool, which also includes a two-DOF worktable.

**Keywords:** dimensional synthesis, dynamic manipulability, parallel manipulator

## 1 INTRODUCTION

Parallel manipulators are leaving academic laboratories and are finding their way in an increasingly larger number of application fields such as machine tool, fast packaging, and medical. A key issue for such use is optimal design as performances of parallel manipulators are sensitive to their dimensioning. Nowadays, high velocity becomes one of the development trends of machine tools. Parallel kinematic machines, which are developed on the basis of parallel manipulators, can easily work in high speed due to their closed kinematic loops [**1**]. Thus, a high-output velocity is very important for parallel manipulators to be applied into parallel kinematic machines. The velocity index [**2**] should also be considered in the dimensional design.

A key issue for problems of manipulator design is dynamic manipulability [**3**, **4**]. The dynamic manipulability is an evaluation on efficiency and easiness for performing required manipulator tasks. Conventionally, dynamic manipulability ellipsoid (DME) [**5**, **6**] and generalized inertia ellipsoid (GIE) [**7**] were used as performance indices to evaluate the dynamic manipulability of a manipulator. DME can deal with weights of directions using maximum required accelerations. Asada [**8**] presented the manipulator dynamics in the task space by constructing a GIE at each point of the workspace. The change in shape and orientation of the GIE from point to point in the workspace was related to the non-linear forces and coupling in the manipulator dynamics.

Besides, some other measures for evaluating dynamic manipulability have been proposed. Graettinger and Krogh [**9**] introduced acceleration radius. For given bounds of joint torques, the corresponding acceleration radius defines the minimum upper bound of the magnitude of end-effector acceleration over the whole workspace. Hashimoto [**10**] used the harmonic mean of the square singular values matrix to evaluate the dynamic manipulability. However, when there is a direction in which the end-effector can be hardly accelerated, it does not always have bad value if it can be easily accelerated in other directions.

**Corresponding author: Institute of Manufacturing Engineering, Department of Precision Instruments, Tsinghua University, Beijing 100084, People's Republic of China. email: wu-j03@mails.tsinghua.edu.cn*

Li *et al.* [**11**] presented the smallest singular value of inertia matrix of a manipulator as the evaluation index when the manipulability in the hardest direction was considered. However, the dynamic manipulability was not considered in all directions. In literatures [**12**] and [**13**], it had demonstrated that the force manipulability ellipsoid was necessary for redundant manipulators.

In this paper, a planar two-DOF parallel manipulator with a high-velocity output ratio is proposed. Based on the kinematics and workspace, the dimensional synthesis based on workspace and velocity output ratio is investigated. By using the virtual work principle, a compact dynamic model is derived. As a result, both local and global performance indices are proposed for evaluating the dynamic manipulability of a parallel manipulator. Based on the parallel manipulator, a four-DOF machine tool, where one translational DOF and one rotational DOF are attached to the worktable, has been developed. The results of the paper are very useful for the design and control of the device.

## 2 STRUCTURE DESCRIPTION

The two-DOF parallel manipulator is shown in Fig. 1. The manipulator is composed of a gantry frame, a moving platform, two active sliders, and two kinematic chains. One chain is built as a parallelogram. Counterweights $P_1$ and $P_2$ (Fig. 1) were added to the manipulator to improve the load capacity and acceleration of the actuator. The sliders are driven independently by two servo motors to slide along the guide ways mounted on the columns, thus the moving platform with a two-DOF purely translational motion in a plane. Links $A_1B_1$ and $A_2B_2$ are the same length

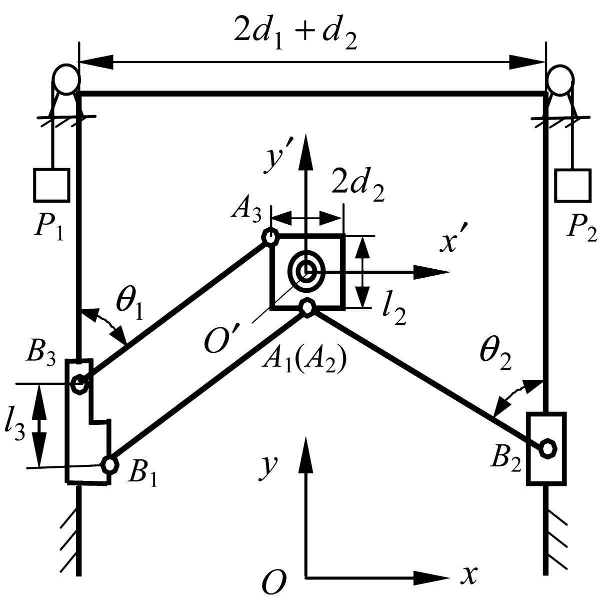


**Fig. 1** Kinematic model of the parallel manipulator

to improve the system performance. The height of the moving platform $l_2$ equals $l_3$, which denotes the height of slider $B_2B_3$.

## 3 KINEMATICS ANALYSIS

### 3.1 Inverse kinematics

As illustrated in Fig. 1, the coordinate system $O-xy$ is attached to the base and a moving coordinate system $O'-x'y'$ is fixed to the moving platform. $2d_1$ is the width between joint point $B_1$ and $B_2$ along the $y$-axis and $2d_2$ is the width of the moving platform.

Let the coordinate of the origin $O'$ be $(x, y)$. According to Fig. 1, the following equation can be obtained

$$\sin\theta_i = \frac{x - x_{Bi}}{l}, \quad \cos\theta_i = \frac{y - l_2/2 - y_{Bi}}{l}, \quad i = 1, 2 \tag{1}$$

From equation (1), the inverse kinematic solutions of the manipulator can be written as

$$q_1 = y_{B1} = y - \frac{l_2}{2} \pm \sqrt{l^2 - (x + d_1)^2} \tag{2a}$$

$$q_2 = y_{B2} = y - \frac{l_2}{2} \pm \sqrt{l^2 - (x - d_1)^2} \tag{2b}$$

It has been investigated that the manipulator experiences an inverse kinematic singularity when one of the three links is horizontal. Direct kinematic singularities occur when links $A_1B_1$ and $A_2B_2$ are collinear. As $2l > 2d_1$, combined singularities cannot occur in this manipulator. In practical applications, both singularities should be avoided. To avoid the inverse kinematic singularity, it is obvious that $0 < |\theta_i| < \pi/2$. Thus, for the configuration as shown in Fig. 1, the '$\pm$' of equation (2) should be only '$-$'.

### 3.2 Jacobian matrix of the inverse kinematic problem

Taking the time derivative of equation (1) leads to

$$\dot{\theta}_i = \frac{\dot{x}}{l\cos\theta_i} \tag{3}$$

$$\dot{q}_i = \dot{y} + \tan\,\theta_i \cdot \dot{x} = \mathbf{J}_i \begin{bmatrix} \dot{x} & \dot{y} \end{bmatrix}^{\mathrm{T}} \tag{4}$$

where $\mathbf{J}_i = \begin{bmatrix} \tan\theta_i & 1 \end{bmatrix}$.

Equation (4) can be rewritten as

$$\dot{q} = \mathbf{J}\dot{p} \tag{5}$$

where $\mathbf{J} = \begin{bmatrix} \mathbf{J}_1^{\mathrm{T}} & \mathbf{J}_2^{\mathrm{T}} \end{bmatrix}^{\mathrm{T}}$.

### 3.3 Velocity index

According to the velocity characteristic of the manipulator, when the manipulator only move along the $y$-axis and $\dot{x} = 0$, it can be concluded that $\dot{q}_1 = \dot{q}_2 = \dot{y}$. Thus, it can be specified that $\dot{y} = 0$ and only discuss the velocity relationship between the input velocity $\dot{q}_i$ of the slider and the output velocity of point $O'$.

Let $k_v(i)$ denote the velocity output ratio, which is the ratio of $\dot{x}$ to $\dot{q}_i$. $k_v(i)$ can be expressed as

$$k_v(i) = \left|\frac{\dot{x}}{\dot{q}_i}\right|, \quad i = 1, 2 \tag{6}$$

Further, let $k_{\mathrm{av}}(i)$ denote the global velocity output ratio, which is the average output velocity of point $O'$ when $x_{\max}$ and $x_{\min}$ are given. $k_{\mathrm{av}}(i)$ can be written as

$$k_{\mathrm{av}}(i) = \frac{\int_{x_{\min}}^{x_{\max}} k_v(i)\,\mathrm{d}x}{x_{\max} - x_{\min}}, \quad i = 1, 2 \tag{7}$$

Although the three links are the same length, it has $k_{\mathrm{av}}(1) = k_{\mathrm{av}}(2)$. For convenience, $k_{\mathrm{av}}$ is used to represent the global velocity ratio.

The velocity output ratio $k_{\mathrm{av}}$ is a global index, which determines the output velocity of a given position when the input velocity is given. For example, when $k_v < 1$ and the position is given, the manipulator input velocity is larger than output velocity. On the contrary, the average output velocity is larger than the average input velocity for $k_v > 1$.

## 4 DIMENSIONAL SYNTHESIS

### 4.1 Workspace of the manipulator

The workspace for the planar two-DOF parallel manipulator is a region of the plane derived by the workspace of reference point $O'$ of the moving platform. Equation (2) can be rewritten as

$$(x + d_1)^2 + \left(q_1 - y + \frac{l_2}{2}\right)^2 = l^2 \tag{8}$$

$$(x - d_1)^2 + \left(q_2 - y + \frac{l_2}{2}\right)^2 = l^2 \tag{9}$$

Therefore, the reachable workspace of reference point $O'$ is the intersection of the subworkspaces associated with two kinematic chains as shown in Fig. 2. Each subspace is the region encircled by two arcs with the radius of $l$. The centres of four arcs are $B_1'(-d_1, q_{1S})$, $B_1''(-d_1, q_{1L})$, $B_2'(d_1, q_{2S})$, and $B_2''(d_1, q_{2L})$, respectively.

The task workspace is a part of the reachable workspace. In practical applications, the task workspace is usually defined as a rectangular area in the reachable workspace. Let the maximum value of the angles $\alpha_1$ and $\alpha_2$ be denoted by $\alpha_{1L}$ and $\alpha_{2L}$. Let $q_{iL}$ and $q_{iS}$ represent the maximum and minimum positions of the slider. Point $O'$ reaches point $Q_3$ when the right slider reaches its lower limit and the value of $\alpha_1$ is the maximum, namely $q_2 = q_{2S}$ and $\alpha_1 = \alpha_{1L}$. Similarly, $O'$ reaches point $Q_2$ when $q_1 = q_{1S}$ and $\alpha_2 = \alpha_{2L}$. A vertical line through $Q_2$ intersects with the upper bound of the reachable workspace at point $Q_1$. $Q_4$ is directly above $Q_3$ (Fig. 2). The region $Q_1Q_2Q_3Q_4$ then makes up the task workspace, which is a rectangle with width $b$ and height $h$.

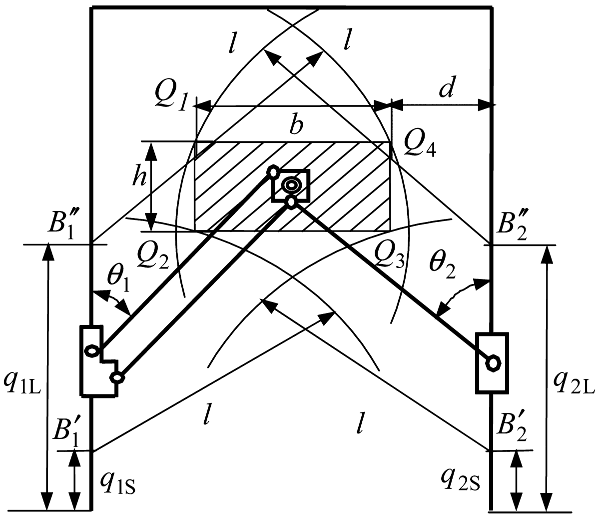


**Fig. 2** Workspace of the parallel manipulator

### 4.2 Dimensional synthesis based on the workspace

The objective of this section is to determine the manipulator parameters for a desired workspace. The scope of dimensional synthesis can be stated as: given $d_2, l_2, b$, and $h$, determine $d_1, l$, and the total moving distance $|q_{iL} - q_{iS}|$ of the slider.

Practically, $d_2$ and $l_2$ should be as small as possible since smaller values of $d_2$ and $l_2$ lead to smaller manipulator volumes. Usually, $d_2$ and $l_2$ depend on the shaft, bearing, and tool dimensions on the moving platform. Therefore, $d_2$ and $l_2$ should be given by the designer.

Based on Fig. 2, when the moving platform reaches the lower limit, the following parametric relationships can be obtained

$$\sin\,\theta_{1S} = \frac{d}{l} \tag{10}$$

$$\sin\,\theta_{2L} = \frac{b + d}{l} \tag{11}$$

When the moving platform moves from point $Q_2$ to $Q_3$ along the $x$-axis, the input, denoted as $y_{d1}$, of each slider should be

$$y_{d1} = l\left(\cos\theta_{1S} - \sin\left(\frac{\pi}{2} - \theta_{2L}\right)\right) \tag{12}$$

From last three equations, it can be seen that if $\theta_{1S} + \theta_{2L} = \pi/2$ then $y_{d1} = b$, which means that the ratio between the input and the output is

$$y_{d1} : b = 1 : 1 \tag{13}$$

Considering the accuracy of the manipulator, it is expected that the effect of the input to output should be smaller, i.e. $y_{d1} : b > 1 : 1$. In such a case, the mirror of the input error to output space will be smaller. If the condition of equation (13) is considered in the design of the manipulator, equations (10) and (11) can be rewritten as

$$d = \frac{b \tan \theta_{1S}}{1 - \tan \theta_{1S}} \tag{14}$$

The parameter $\theta_{1S}$ can have different values, which will depend on the designer's demand. But if $\theta_{1S}$ is very small, the configuration of the manipulator, shown in Fig. 2, will near the singularity. Other parameters $d_1$, $l$, and $|q_{iL} - q_{iS}|$ will be obtained as

$$l = \frac{b+d}{\sin \theta_{2L}}, \quad d_1 = \frac{b+2d}{2} \tag{15}$$

$$|q_{iL} - q_{iS}| = y_{d1} + h \tag{16}$$

Therefore, if $b = 500\,\text{mm}$, $h = 400\,\text{mm}$, $\theta_{1S} = 15°$, $d_2 = 100\,\text{mm}$, and $l_2 = 200\,\text{mm}$, $d_1 = 433\,\text{mm}$, $l = 707.1\,\text{mm}$, and $|q_{iL} - q_{iS}| = 900\,\text{mm}$, which are the design results from the desired workspace alone, can be obtained. As one knows, in the process of dimensional design, the workspace cannot be the only index to be considered. It cannot guarantee a manipulator that might satisfy the workspace requirement could be suitable for a particular application. To obtain a large velocity output ratio, the global velocity index $k_{av}$ should be also considered in this process.

### 4.3 Improved design based on the global velocity index

In order to determine $k_{av}$, $x_{max}$, and $x_{min}$ should be determined. $x_{max}$ and $x_{min}$ can be expressed as

$$x_{min} = -\frac{b}{2} \tag{17}$$

$$x_{max} = \frac{b}{2} \tag{18}$$

The task workspace of the parallel manipulator is designed as a rectangle of $b = 500\,\text{mm}$ in width and $h = 400\,\text{mm}$ in height. According to equation (7), the relationship between $k_{av}$ and $\theta_1$ is determined. $k_{av}$ descends when $\theta_1$ varies from 0 to 90°. The larger $k_{av}$, the larger the output velocity of the manipulator. Thus, a smaller $\theta_1$ is expected. $\theta_1$ cannot get a very small value since the manipulator experiences a singularity at $\theta_1 = 0$. With respect to singularities, the larger the value of $\theta_1$, the better the performance of the manipulator. However, the larger one will result in larger volume of the manipulator and smaller value of $k_{av}$. Considering that $k_{av}$ has a small range when the value of $\alpha_1$ is $> 10°$, in this paper, the minimum value of $\theta_1$ as $\theta_{1S} = 10°$ is specified. Accordingly, $\theta_{2L} = 80°$. Then, $d_1$, $l$, and $|q_{iL} - q_{iS}|$ are determined by equations (15) and (16), respectively. The main parameters are shown in Table 1.

**Table 1** Optimization results

| Parameter | Value |
|---|---|
| $l$ | 616.4 mm |
| $d_2$ | 100 mm |
| $\|q_{iL} - q_{iS}\|$ | 900 mm |
| $d_1$ | 357 mm |
| $l_2$ | 200 mm |
| $k_{av}$ | 1.05 |

By combining the two-DOF parallel manipulator with a worktable that has a translational DOF in the $z$-direction (along the spindle) and a rotational DOF about the $y$-axis, a four-DOF hybrid machine tool is created. The machine tool was built by Tsinghua University. The assembly drawing is shown in Fig. 3.

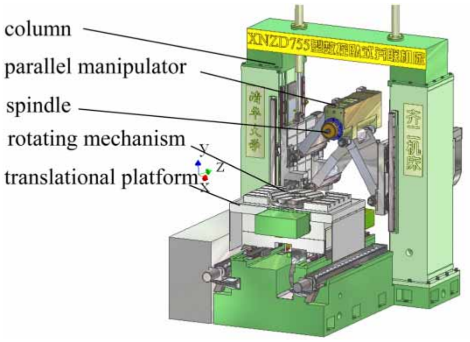


**Fig. 3** Assembly drawing of the machine

## 5 DYNAMIC MODELLING

The virtual work principle is utilized to derive the dynamic model. In order to write the dynamic model in a standard form, the inertial force and moment of each moving part are decomposed into two terms, respectively. One term is related to the acceleration of the moving platform, and the other is out of the platform acceleration.

### 5.1 Partial velocity and partial angular velocity matrix

In order to obtain a more compact form of the dynamic model, the virtual work principle is employed to derive the dynamic model. Thus, the partial velocity and partial angular velocity matrices [**14**], which are used in dynamic modelling, should be determined first. To find the partial velocity matrix, a pivotal point should be selected to have the simplest form of velocity, so that the determination of partial velocity matrix can be most efficient. For example, the points $B_1$ and $B_2$ are selected as the pivotal point of the left and right sliders, and $B_i$ is the pivotal point of link $A_iB_i$ ($i = 1, 2, 3$). The mass centres of the counterweight and the moving platform are regarded as their pivotal points, respectively. Then, the partial velocity matrix of each pivotal point and partial angular velocity matrix of each moving part can be computed, respectively.

Since the slider has only the translational capability, the partial angular velocity matrix can be expressed as

$$\mathbf{G}_{i1} = 0 \tag{19}$$

According to equation (4), the partial velocity matrix of point $B_i$ is given by

$$\mathbf{H}_{i1} = \begin{bmatrix} 0 & 1 \end{bmatrix}^{\mathrm{T}} \mathbf{J}_i, \quad i = 1, 2 \tag{20}$$

Based on equation (3), the partial angular velocity matrix of link $A_iB_i$ and partial velocity matrix of point $B_i$ can be written as

$$\mathbf{G}_{i2} = \begin{bmatrix} \dfrac{1}{\cos\ \theta_i \cdot l} & 0 \end{bmatrix} \tag{21}$$

$$\mathbf{H}_{i2} = \mathbf{H}_{i1} \tag{22}$$

While the counterweight is connected to the slider, the velocity of the counterweight is the negative of that of the slider. Then, the partial angular velocity matrix and partial velocity matrix of the mass centre of the counterweight can be expressed as

$$\mathbf{G}_{i3} = 0, \quad \mathbf{H}_{i3} = \begin{bmatrix} 0 & -1 \end{bmatrix}^{\mathrm{T}} \mathbf{J}_i \tag{23}$$

Owing to the parallelogram structure of kinematic chain $A_1B_1B_3A_3$, the motion of link $A_3B_3$ is the same as that of link $A_1B_1$. Thus, the partial velocity matrix of point $B_3$ and the partial angular velocity matrix of link $A_3B_3$ are the same as those of point $B_1$ and link $A_1B_1$. Namely

$$\mathbf{G}_4 = \mathbf{G}_{12}, \quad \mathbf{H}_4 = \mathbf{H}_{12} \tag{24}$$

Considering that the moving platform cannot rotate, the partial angular velocity matrix of the moving platform and partial velocity matrix of point $O'$ are given by

$$\mathbf{G}_N = 0 \tag{25}$$

$$\mathbf{H}_N = \begin{bmatrix} 1 & 0 \\ 0 & 1 \end{bmatrix} \tag{26}$$

### 5.2 Inertial force and inertial moment of moving part

Taking the time derivative of equations (3) and (4) leads to

$$\ddot{\theta}_i = \frac{\ddot{x}}{l \cos\ \theta_i} + \frac{\dot{x}^2 \sin\ \theta_i}{l^2 \cos^3\ \theta_i} \tag{27}$$

$$\ddot{q}_i = \ddot{y} + \tan\ \theta_i \ddot{x} + \frac{\dot{x}\dot{\theta}_i}{\cos^2\ \theta_i} \tag{28}$$

Thus, the acceleration of point $B_i$ is determined by

$$\mathbf{a}_{\mathrm{B}i} = \begin{bmatrix} 0 & 1 \end{bmatrix}^{\mathrm{T}} \ddot{q}_i \tag{29}$$

Utilizing the Newton–Euler formulation, the inertial force and moment of each moving part about the pivotal point can be determined. Here, it is assumed that $m_{i1}$, $m_{i2}$, $m_{i3}$, $m_4$, and $m_N$ are the masses of the slider, links $A_iB_i$ ($i = 1, 2$), the counterweight, link $A_3B_3$, and the moving platform, respectively, $\mathbf{g}$ the gravitational acceleration vector and $\mathbf{g} = \begin{bmatrix} 0 & -9.8 \end{bmatrix}^{\mathrm{T}} \mathrm{m/s^2}$.

The inertial force and moment of the slider about point $B_i$ can be expressed as

$$\mathbf{F}_{i1} = -\mathbf{m}_{i1}(\mathbf{a}_{\mathrm{B}i} - \mathbf{g}) = -m_{i1} \begin{bmatrix} 0 \\ \ddot{y} + \tan\theta_i \ddot{x} \end{bmatrix} + \tilde{\mathbf{F}}_{i1} \tag{30}$$

$$M_{i1} = 0 \tag{31}$$

where

$$\tilde{\mathbf{F}}_{i1} = -m_{i1} \begin{bmatrix} 0 \\ \frac{\dot{x}\dot{\theta}_i}{\cos^2\theta_i} \end{bmatrix} + m_{i1}\mathbf{g}$$

The inertial force and moment of link $A_iB_i$ ($i = 1, 2$) about point $B_i$ can be expressed as

$$\begin{aligned} \mathbf{F}_{i2} &= -m_{i2}\left(\mathbf{a}_{\mathrm{B}i} + s_{i2}\ddot{\theta}_i \mathbf{E} \begin{bmatrix} \sin\theta_i \\ -\cos\theta_i \end{bmatrix} - s_{i2}\,\dot{\theta}_i^2 \begin{bmatrix} \sin\theta_i \\ -\cos\theta_i \end{bmatrix} - \mathbf{g}\right) \\ &= -m_{i2} \begin{bmatrix} s_{i2}\ddot{x}/l \\ \ddot{y} + \tan\theta_i \ddot{x} + s_{i2}/l \cdot \tan\theta_i \ddot{x} \end{bmatrix} + \tilde{\mathbf{F}}_{i2} \end{aligned} \tag{32}$$

$$\begin{aligned} M_{i2} &= -\ddot{\beta}_i I_{i2} + m_{i2}s_{i2} \begin{bmatrix} \sin\theta_i & -\cos\theta_i \end{bmatrix} \mathbf{E}(a_{\mathrm{B}i} - \mathbf{g}) \\ &= \frac{-m_{i2}ls_{i2}\sin^2\theta_i - I_{i2}}{l\cos\theta_i}\ddot{x} - m_{i2}s_{i2}\sin\theta_i \ddot{y} + \tilde{M}_{i2} \end{aligned} \tag{33}$$

where

$$\mathbf{E} = \begin{bmatrix} 0 & -1 \\ 1 & 0 \end{bmatrix}$$

$$\tilde{\mathbf{F}}_{i2} = m_{i2} \begin{bmatrix} \dfrac{s_{i2} \cdot \dot{x}^2 \sin\theta_i}{l^2 \cos^2\theta_i} \\ - s_{i2} \sin\theta_i \cdot \dot{\theta}_i^2 \\ \dfrac{\dot{x}\dot{\theta}_i}{\cos^2\theta_i} + \dfrac{s_{i2}\dot{x}^2 \sin^2\theta_i}{l\cos^3\theta_i} \\ + s_{i2} \cos\theta_i \cdot \dot{\theta}_i^2 \end{bmatrix} + m_{i2}\mathbf{g},$$

$$\tilde{M}_{i2} = \frac{m_{i2}s_{i2}l^2 \cos\theta_i \sin\theta_i \dot{x}\dot{\theta}_i - I_{i2} \sin\theta_i \dot{x}^2}{l^2\cos^3\theta_i} - 9.8 \cdot m_{i2}s_{i2} \sin\theta_i$$

$\mathbf{a}_{Bi}$ is the acceleration of point $B_i$, $s_{i2}$ is the distance between the mass centre of link $A_iB_i$ and point $B_i$, and $I_{i2}$ is the moment of inertia of link $A_iB_i$ about point $B_i$.

The inertial force and moment of the counterweight about its mass centre can be written as

$$\mathbf{F}_{i3} = -m_{i3}(\mathbf{a}_{Pi} - \mathbf{g}) = m_{i3} \begin{bmatrix} 0 \\ \ddot{y} + \tan\theta_i \ddot{x} \end{bmatrix} + \tilde{\mathbf{F}}_{i3} \quad (34)$$

$$M_{i3} = 0 \quad (35)$$

where

$$\tilde{\mathbf{F}}_{i3} = m_{i3} \begin{bmatrix} 0 \\ \frac{\dot{x}\dot{\theta}_i}{\cos^2\theta_i} \end{bmatrix} + m_{i3}\mathbf{g}.$$

Since links $A_3B_3$ and $A_1B_1$ have the same motion, the inertial force and moment of link $A_3B_3$ are the same as those of link $A_1B_1$. Thus, the inertial force and moment of link $A_3B_3$ are determined by

$$\mathbf{F}_4 = \mathbf{F}_{12} \quad (36)$$

$$M_4 = M_{12} \quad (37)$$

The inertial force and moment of the moving platform about point $O'$ can be expressed as

$$\mathbf{F}_N = -m_N(\mathbf{a} - \mathbf{g}) \quad (38)$$

$$M_N = 0 \quad (39)$$

## 5.3 Dynamic model

Based on the virtual work principle, the dynamic formulation of the parallel manipulator can be expressed as

$$\mathbf{J}^{\mathrm{T}}\boldsymbol{\tau} + \sum_{i=1}^{2}\sum_{j=1}^{3} \begin{bmatrix} \mathbf{H}_{ij}^{\mathrm{T}} & \mathbf{G}_{ij}^{\mathrm{T}} \end{bmatrix} \begin{bmatrix} \mathbf{F}_{ij} \\ M_{ij} \end{bmatrix} + \begin{bmatrix} \mathbf{H}_N^{\mathrm{T}} & \mathbf{G}_N^{\mathrm{T}} \end{bmatrix} \begin{bmatrix} \mathbf{F}_N \\ M_N \end{bmatrix} + \begin{bmatrix} \mathbf{H}_4^{\mathrm{T}} & \mathbf{G}_4^{\mathrm{T}} \end{bmatrix} \begin{bmatrix} \mathbf{F}_4 \\ M_4 \end{bmatrix} = \mathbf{0} \quad (40)$$

where $\boldsymbol{\tau} = \begin{bmatrix} F_1 & F_2 \end{bmatrix}^{\mathrm{T}}$. Equation (40) can be rewritten as

$$\boldsymbol{\tau} = (\mathbf{J}^{\mathrm{T}})^{-1}\mathbf{Ma} + \mathbf{N} \quad (41)$$

where

$$\mathbf{M} = -\sum_{i=1}^{2} \left( \begin{array}{c} -m_{i1}\begin{bmatrix} \tan^2\theta_i & \tan\theta_i \\ \tan\theta_i & 1 \end{bmatrix} \\ -m_{i2}\begin{bmatrix} (1+s_{i2}/l)\tan^2\theta_i & \tan\theta_i \\ (1+s_{i2}/l)\tan\theta_i & 1 \end{bmatrix} \\ -\begin{bmatrix} \dfrac{m_{i2}s_{i2}l\sin^2\theta_i + I_{i2}}{l^2\cos^2\theta_i} & \dfrac{m_{i2}s_{i2}\sin\theta_i}{l\cos\theta_i} \\ 0 & 0 \end{bmatrix} \\ -m_{i3}\begin{bmatrix} \tan^2\theta_i & \tan\theta_i \\ \tan\theta_i & 1 \end{bmatrix} \end{array} \right) + m_{12}\begin{bmatrix} (1+s_{12}/l)\tan^2\theta_1 & \tan\theta_1 \\ (1+s_{12}/l)\tan\theta_1 & 1 \end{bmatrix} + m_N\begin{bmatrix} 1 & 0 \\ 0 & 1 \end{bmatrix}$$

$$\mathbf{N} = -\sum_{i=1}^{2} \left( \begin{array}{c} \begin{bmatrix} 0 & \tan\theta_i \\ 0 & 1 \end{bmatrix}\tilde{\mathbf{F}}_{i1} + \begin{bmatrix} 0 & \tan\theta_i \\ 0 & 1 \end{bmatrix}\tilde{\mathbf{F}}_{i2} \\ + \begin{bmatrix} 1/(l\cos\theta_i) \\ 0 \end{bmatrix}\tilde{M}_{i2} + \begin{bmatrix} 0 & -\tan\theta_i \\ 0 & -1 \end{bmatrix}\tilde{\mathbf{F}}_{i3} \end{array} \right) - \begin{bmatrix} 0 & \tan\theta_1 \\ 0 & 1 \end{bmatrix}\tilde{\mathbf{F}}_{12} - m_N\mathbf{g}$$

consists of the centrifugal, coriolis, and gravitational forces.

# 6 DYNAMIC MANIPULABILITY

## 6.1 Performance indices

Although there are many performance indices for evaluating the dynamic manipulability, DME and GIE were conventionally used to evaluate the dynamic performance of a manipulator. Both the GIE and the DME are based on the relationship between the generalized inertia force of the end-effector and the generalized inertia torques of joints. As addressed in reference [**6**], the dynamic performance of a high-speed manipulator can be represented by the degree of arbitrariness of changing the acceleration on the actuated joint force. Thus, rewriting equation (41) in a unified form by neglecting $\mathbf{N}$, leads to

$$\boldsymbol{\tau} \approx (\mathbf{J}^{\mathrm{T}})^{-1}\mathbf{Ma} \quad (42)$$

where $(\mathbf{J}^{\mathrm{T}})^{-1}\mathbf{M}$ is the inertia matrix.

Based on the GIE, it can be concluded that the moving platform can be easily accelerated in the direction of major axis of this ellipsoid. In the direction of minor axis, it can be hardly accelerated. The maximum and minimum singular values of inertia matrix reflect the lengths of the principal axes of the inertia ellipsoid. If the lengths of the principal axes are the same, the accelerating performance is isotropic. The difference between the lengths of major and minor axes stands for the anisotropy of the accelerating performance.

In the dynamic optimum design, if the issue that the accelerating/decelerating capabilities along all directions should be more isotropic is considered, the condition number of the inertia matrix in the dynamic equation, i.e. $\kappa_D$, is proposed to quantify the dynamic manipulability of manipulators. $\kappa_D$ is defined as

$$1 \leqslant \kappa_D = \frac{\sigma_2}{\sigma_1} \leqslant \infty \tag{43}$$

$\kappa_D$ can evaluate the dynamic manipulability when the difference between the easiest direction and the hardest one is the main issue. Considering that $\kappa_D$ varies in different configurations of the manipulator, one global index, similar to that introduced in references [**11**] and [**15**], is proposed as

$$\bar{\eta}_D = \frac{\int_{W_t} \kappa_D \mathrm{d}W_t}{\int_{W_t} \mathrm{d}W_t} \tag{44}$$

### 6.2 Dynamic manipulability of the manipulator

Let the moving platform move from the point $q_0 = [x_0 \quad y_0]^T\, m$ to $q_1 = [x_1 \quad y_1]^T\, m$ through accelerating, constant velocity, and decelerating phases, and the accelerating time and the decelerating time is equal. The accelerating time $T_0$ is given by

$$T_0 = T_f - |q_1 - q_0|/V_{max} \tag{45}$$

As an example to investigate the driving forces and dynamic manipulability, the inertial parameters and motion parameters of the manipulator are given in Tables 2 and 3. The masses of two counterweights are equal, and each is half of the masses of all moving parts (no including counterweights). In Table 3, $a_S$ is the acceleration in the simulation. The driving forces are given in Fig. 4. It can be seen that the driving forces change smoothly in the simulation process.

Figure 5 shows the GIE. The axes of ellipsoid lie in the directions of the eigenvectors of inertia matrix. The moving platform can possess a maximum (minimum) acceleration in the direction of the major (minor) axis of the ellipsoid. The larger the area of ellipsoid is, the larger the output acceleration is. Figure 6 is geometrical mean value of $\kappa_D$ in $W_t$ It can be seen that the dynamic manipulability is more isotropic in the centre than at the peripheries of the workspace.

**Table 2** Inertial parameters

| Parameter | Value |
|---|---|
| $m_{11}$ | 250 kg |
| $m_{21}$ | 198 kg |
| $m_{12}$ | 80 kg |
| $m_{22}$ | 80 kg |
| $m_{13}$ | 462 kg |
| $m_{23}$ | 462 kg |
| $m_4$ | 80 kg |
| $m_N$ | 236 kg |
| $I_{12}$ | 11.3 kg m$^2$ |
| $I_{22}$ | 11.3 kg m$^2$ |

**Table 3** Motion parameters

| Parameters | Values |
|---|---|
| $x_0$ | −0.25 m |
| $y_0$ | 0.5 m |
| $\lvert v_{max}\rvert$ | 1 m/s |
| $x_1$ | 0.25 mm |
| $y_1$ | 0.5 m |
| $\lvert a_s\rvert$ | 6.67 m/s$^2$ |

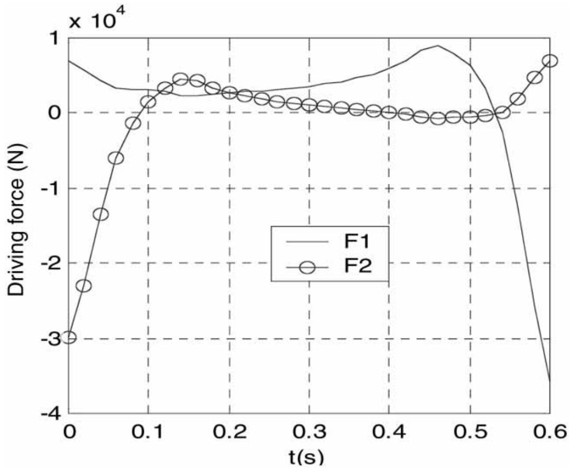


**Fig. 4** Driving forces

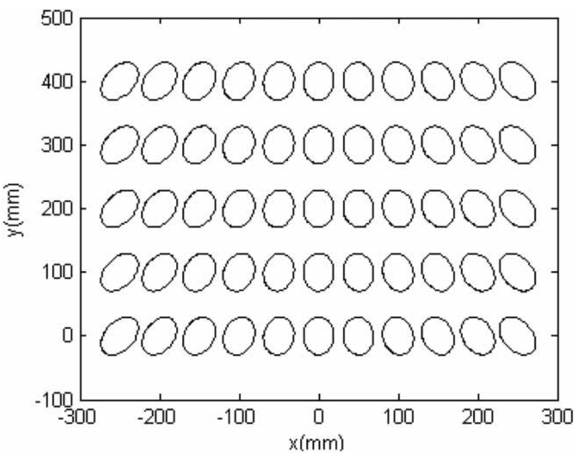


**Fig. 5** Distribution of generalized inertia ellipsoid

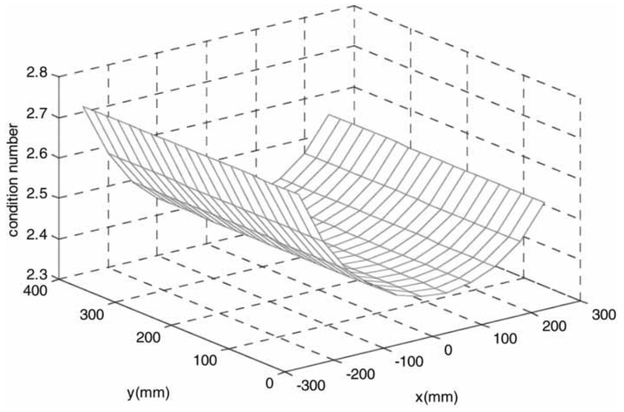


**Fig. 6** $\bar{\eta}_D$ in the workspace

### 6.3 Dynamic manipulability of a manipulator with symmetrical structure

In order to investigate the validity of the proposed performance indices $\kappa_D$ and $\bar{\eta}_D$ for evaluating the dynamic manipulability of a manipulator, it is assumed that an additional link $A_4B_4$ is inserted in such a way that the right link in Fig. 2 is extended to a parallelogram. The manipulator studied in this paper would be symmetrical, and it is similar to the manipulator proposed in literature [**16**]. $\bar{\eta}_D$ is used to evaluate the dynamic manipulability of the new manipulator.

Figure 7 is the distribution of $\bar{\eta}_D$ of the two-DOF parallel manipulator with a symmetrical structure. From Fig. 7, it can be seen that the accelerating capability of the point in the $y$-axis is maximum along the $y$-direction and minimum along the $x$-direction. In the $y$-axis, $\kappa_D$ is smallest and the dynamic manipulability is most isotropic. Further, the proposed index $\bar{\eta}_D$ is symmetrical about the $y$-axis, which is in accordance with the structural symmetry of the manipulator with an additional link $A_4B_4$. Thus, it can be concluded that $\kappa_D$ and $\bar{\eta}_D$ are effective for evaluating the dynamic manipulability of a manipulator.

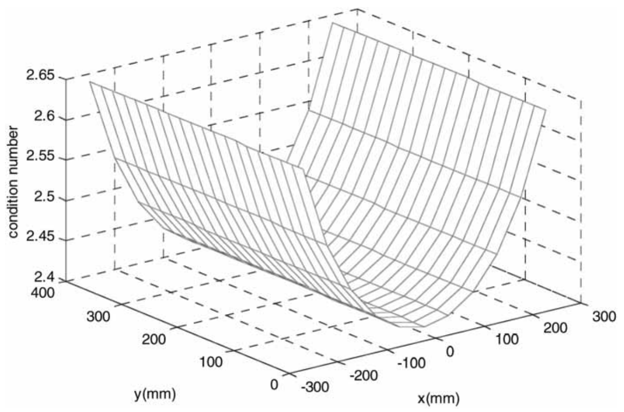


**Fig. 7** $\bar{\eta}_D$ for the manipulator with link $A_4B_4$

Since the workspace of the manipulator is symmetrical, the machining performance and efficiency would be best if $\bar{\eta}_D$ is symmetrical with respect to the $y$-axis. Thus, a symmetrical structure would be ideal for the manipulator. Considering the simplicity and internal force problem caused by the virtual-constrain of the symmetrical structure, the manipulator studied in this paper was finally designed as a non-symmetrical manipulator. However, some new manipulators [**16**, **17**] after the manipulator are constructed with symmetrical structure.

## 7 CONCLUSIONS

The dimensional synthesis and dynamic manipulability of a planar two-DOF parallel manipulator have been investigated in this article. From this investigation, the following conclusions can be drawn:

1. The dimensional synthesis is performed by two steps. First, a design result is obtained with respect to a desired workspace. Then, the results are improved by considering $k_{av}$.
2. $\kappa_D$, $\bar{\eta}_D$, and $\tilde{\eta}_D$ are presented as local and global performance indices to evaluate the dynamic manipulability of a manipulator, respectively. The dynamic manipulability of the two-DOF parallel manipulator is more isotropic in the centre than at the peripheries of the workspace. Furthermore, $\bar{\eta}_D$ is not symmetrical about the $y-$axis due to the structural asymmetry of the manipulator.
3. The proposed parallel manipulator is incorporated into a four-DOF hybrid machine tool to demonstrate its applicability.

## ACKNOWLEDGEMENTS

This work is supported by the National Nature Science Foundation of China (Grant No. 50775117 and 50775125), Scientific and Technical Supporting Program (Grant No. 2006BAF01B09), and the 973 Program of China (Grant No. 2004CB318007 and 2006CB705400).

## REFERENCES

1 **Weck, M.** and **Staimer, D.** Parallel kinematic machine tools-current state and future potentials. *CIRP Ann. Manuf. Technol.*, 2002, **51**(2), 671–683.

2 **Liu, X.-J., Wang, J.-S.,** and **Pritschow, G.** Performance atlases and optimum design of planar 5R symmetrical parallel mechanisms. *Mech. Mach. Theory*, 2006, **41**(2), 119–144.

3 **Tadokoro, S., Kimura, I.,** and **Takamori, T.** A measure for evaluation of dynamic dexterity based on a stochastic interpretation of manipulator motion. In fifth International Conference on Advanced Robotics, Pisa, Italy, 1991, pp. 509–514.
4 **Doty, K. L., Melchiorri, C., Schwartz, E. M.,** and **Bonivento, C.** Robot manipulability. *IEEE Trans. Robot. Automat.*, 1995, **11**(3), 462–468.
5 **Yoshikawa, T.** Dynamic manipulability of robot manipulators. *J. Robot. Syst.*, 1985, **2**(1), 113–124.
6 **Yoshikawa, T.** Manipulability of robotic mechanisms. *Int. J. Robot. Res.*, 1985, **4**(2), 3–9.
7 **Asada, H.** and **Youcef-Toumi, K.** Analysis and design of a direct-drive arm with a five-bar-link parallel drive mechanism. *ASME J. Dyn. Syst. Meas. Control*, 1984, **106**(3), 225–230.
8 **Asada, H.** A geometrical representation of manipulator dynamics and its application to arm design. *J. Dyn. Syst. Meas. Control*, 1983, **105**(3), 131–135.
9 **Graettinger, T. J.** and **Krogh, B. H.** The acceleration radius: a global performance measure for robotic manipulators. *IEEE J. Robot. Autom.*, 1988, **4**(1), 60–69.
10 **Hashimoto, R.** Harmonic mean type manipulatability index of robotic arms. *Trans. Soc. Instrum. Control Eng.*, 1985, **21**(12), 1351–1353.
11 **Li, M., Huang, T., Mei, J., Zhao, X., Chetwynd, D.G., Hu, S.J.** Dynamic formulation and performance comparison of the 3-DOF modules of two reconfigurable PKM-the Tricept and the TriVariant. *ASME J. Mech. Des.*, 2005, **127**(6), 1129–1136.
12 **Chiacchio, P., Bouffard-Vercelli, Y.,** and **Pierrot, F.** Force polytope and force ellipsoid for redundant manipulators. *J. Robot. Syst.*, 1997, **14**(8), 613–620.
13 **Chiacchio, P.** New dynamic manipulability ellipsoid for redundant manipulators. *Robotica*, 2000, **18**(4), 381–387.
14 **Zhang, C. D.** and **Song, S. M.** An efficient method for inverse dynamics of manipulators based on the virtual work principle. *J. Robot. Syst.*, 1993, **10**(5), 605–627.
15 **Gosselin, C. M.** and **Angeles, J.** A global performance index for the kinematic optimization of robotic manipulators. *ASME J. Mech. Des.*, 1991, **113**(3), 220–226.
16 **Wu, J., Wang, J., Li, T.,** and **Wang, L.** Dynamic analysis of the 2-DOF planar parallel manipulator of a heavy duty hybrid machine tool. *Int. J. Adv. Manuf. Technol.*, 2007, **34**(3–4), 413–420.
17 **Liu, X.-J., Wang, Q.-M.,** and **Wang, J.** Kinematics, dynamics and dimensional synthesis of a novel 2-DOF translational manipulator. *J. Intel. Robot. Syst.*, 2004, **41**(4), 205–224.

## APPENDIX

### Notation

| | |
|---|---|
| $a_{Pi}$ | acceleration of the counterweight |
| $a$ | acceleration of the moving platform |
| $d$ | distance from the right column to the right bound |
| $l$ | length of the link |
| $F_1$ | driving force that act on the left slider |
| $F_2$ | driving force that act on the right slider |
| $\mathbf{J}$ | Jacobian matrix |
| $\dot{p} = [\dot{x} \quad \dot{y}]^T$ | velocity of the moving platform |
| $\dot{q} = [\dot{q}_1 \quad \dot{q}_2]^T$ | slider velocity |
| $T_f$ | total moving time |
| $V_{max}$ | maximum velocity of the moving platform |
| $W_t$ | task workspace of a manipulator in which the dynamic manipulability is evaluated |
| $x_{Bi}$ | $x$-coordinate of point $B_i$ |
| $x_{max}$ | $x$-axis maximum reachable coordinates of point $O'$ |
| $x_{min}$ | $x$-axis minimum reachable coordinates of point $O'$ |
| $y_{Bi}$ | $y$ coordinate of point $B_i$ |
| $\theta_i$ | angle between link $A_iB_i$ and the vertical axis parallel to the $y$-axis |
| $\theta_{1S}$ | minimum value of $\theta_1$ |
| $\sigma_1$ | minimum singular value of the inertia matrix with a given posture |
| $\sigma_2$ | maximum singular value of the inertia matrix with a given posture |